D. T. Klier | M. U. Kumke

Upconversion $NaYF_4$:Yb:Er nanoparticles co-doped with Gd^{3+} and Nd^{3+} for thermometry on the nanoscale

Suggested citation referring to the original publication:
RSC Adv. 5 (2015), 67149–67156
DOI http://dx.doi.org/10.1039/C5RA11502G

RSC Advances

PAPER

View Article Online
View Journal | View Issue

Cite this: *RSC Adv.*, 2015, **5**, 67149

Upconversion $NaYF_4$:Yb:Er nanoparticles co-doped with Gd^{3+} and Nd^{3+} for thermometry on the nanoscale†

D. T. Klier‡ and M. U. Kumke‡

Received 16th June 2015
Accepted 30th July 2015

DOI: 10.1039/c5ra11502g

www.rsc.org/advances

In the present work, the upconversion luminescence properties of oleic acid capped $NaYF_4$:Gd^{3+}:Yb^{3+}:Er^{3+} upconversion nanoparticles (UCNP) with pure β crystal phase and Nd^{3+} ions as an additional sensitizer were studied in the temperature range of 288 K < *T* < 328 K. The results of this study showed that the complex interplay of different mechanisms and effects, causing the special temperature behavior of the UCNP can be developed into thermometry on the nanoscale, *e.g.* to be applied in biological systems on a cellular level. The performance was improved by the use of Nd^{3+} as an additional dopant utilizing the cascade sensitization mechanism in tri-doped UCNP.

1. Introduction

Temperature is a fundamental parameter of key importance in many different fields of science and technology. Respective sensors are widely used in on a daily basis in climate and marine research as well as in chemistry, biology, metrology, and medicine.[1–3] It is estimated that the share of temperature sensors amounts to as much as 75–80% of the world's sensor market.[4] Indeed, current technological demands like microfluidics or nano medicine have reached a point at which a spatial resolution on the submicron scale is needed.[5] For example the mapping of the temperature in living cells, *i.e.* cancer cells compared to normal tissue have a higher temperature due to the increased metabolic activity, which strongly improves the perception of their pathology and physiology and in turn can help to optimize diagnosis and therapeutic approaches, *e.g.*, hydrothermal treatment or photodynamic therapy. In particular a thermometer capable of subdegree temperature resolution as well as integration on a cellular level could provide a powerful new tool in many areas of biochemical and biophysical research.[5,6] Many promising approaches for local temperature sensing are being explored at present such as Raman spectroscopy,[6] scanning probe microscopy[6] and luminescent based measurements using organic dyes,[7,8] nanomaterials[9–11] such as quantum dots (QD) or proteins.[8] Many of these already existing methods suffer on several drawbacks such as low sensitivity, low reproducibility or systematic errors due to fluctuations in the luminescence rate or local chemical environment.[10]

Our approach to nanoscale thermometry uses luminescence upconversion nanoparticles (UCNP), which are suitable for investigation in different biological matrices. The UCNP are excited with light in the near infrared range (NIR), where interferences from background fluorescence can be neglected.[12] In the chosen excitation wavelength range between 795 nm < λ_{ex} < 976 nm many biological matrices are nearly transparent.[13] Consequently, the penetration depth in this spectral range is very high for a human skin or in blood (see Fig. 1) and a high sensitivity in sensing applications without additional sample preparations can be established.[13] One of the first promising approaches for upconversion nanoparticle based thermometry

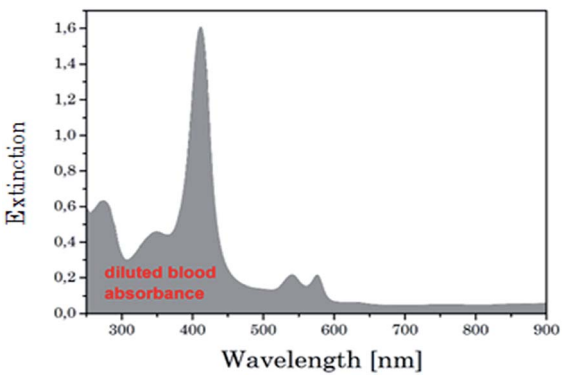

Fig. 1 Absorption spectra of diluted blood.

University of Potsdam, Department of Chemistry (Physical Chemistry), Karl-Liebknecht-Str. 24-25, 14476 Potsdam, Germany. E-mail: kumke@uni-potsdam.de

† Electronic supplementary information (ESI) available: DLS analysis of $UCNP_{Nd,OA}$ $NaYF_4$:Yb/Er (17/3 mol%) with a Nd^{3+} dopant concentration of 2 mol% and UCNP. Excitation emission matrices of $UCNP_{Nd}$ are shown. Power dependence of the Er^{3+} transitions G1, G2 and R of oleic acid capped UCNP at different excitation wavelength are shown as well as the temperature dependence of the upconversion luminescence of $UCNP_{Nd}$ dissolved in water at different irradiation wavelength and thermostat temperature over time. See DOI: 10.1039/c5ra11502g

‡ These authors equally contributed to this study.

on nanoscale was developed by Zink *et al.*[14] They used a dual core (made of UCNP and smaller superparamagnetic nanocrystal) mesoporous silica nano-particle that acted as nanothermometer as well as nanoheater. An in-depth investigation of the potential of UCNP as nanothermometer was carried out by Wolfbeis *et al.* using different lanthanide combination and capping agents.[15] Here, the best results were found for $NaYF_4$:Yb^{3+}:Er^{3+} core/shell nanoparticles. Moreover, UCNP can be developed into multimodal probes, *e.g.*, with additives like gadolinium (Gd^{3+}) ions UCNP can be used for magnet resonance imaging or with the appropriate functionalization for optical imaging or assay applications.[16–18] Apart from the excitation at $\lambda_{ex} = 976$ nm Han *et al.* report on UCNP with additional Nd^{3+} doping which could be excited at $\lambda_{ex} = 800$ nm. This type of UCNP showed a better biocompatibility due to lower impact on biological tissues and a higher penetrability for the excitation light.[19]

In the present work, the potential of oleic acid-capped $NaYF_4$:Gd^{3+}:Yb^{3+}:Er^{3+} upconversion nanoparticles (UCNP) for thermometry on nanometer scales was studied in the temperature range of 288 K < T < 328 K. Both, the overall luminescence intensity and the ratio of luminescence bands were found to be highly sensitive on temperature. For the temperature determination the intensity ratio of the luminescence signal in the green Er^{3+} luminescence bands ($^2H_{11/2} \rightarrow {}^4I_{15/2}$ (G1) and $^4S_{3/2} \rightarrow {}^4I_{15/2}$ (G2)) was used. The relative sensitivity (S_r) with 1.49% K^{-1} of the UCNP under investigation is one of the highest S_r value which found in literature for $NaYF_4$:Yb^{3+}:Er^{3+} type nanoparticles or other host lattices like $GdVO_4$:Yb^{3+}:Er^{3+} or $Na_2Y_2B_2O_7$:Yb^{3+}:Tm^{3+}.[20,21]

The overlapping of the excitation light at $\lambda_{ex} = 976$ nm with the absorption of water (see Fig. 2), which may induce heating damage in cells and tissues, is a drawback *e.g.*, for nanoparticle-based imaging or for deep tissue imaging (this experiments require high excitation energy and long-term excitation). To overcome this limitation, Nd^{3+} was used as additional lanthanide. Nd^{3+} has an absorption maximum around $\lambda = 800$ nm, which can be used for the initial excitation of the UCNP. At this excitation wavelength the intrinsic water absorption is one order of magnitude lower compared to $\lambda_{ex} = 976$ nm resulting in less heating of the sample by the laser irradiation (see Fig. 2). Subsequently a better biocompatibility and higher penetration depth in aqueous systems can be envisaged. Colloidal tri-doped (Yb^{3+}, Er^{3+} and Gd^{3+} ions) UCNPs with Nd^{3+} were successfully generated and optimized for maximum upconversion efficiency with an excitation wavelength of $\lambda_{ex} = 800$ nm.

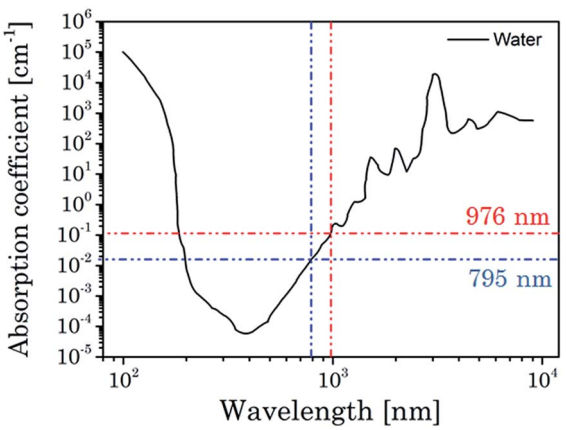

Fig. 2 Absorption coefficient of water in a spectral range of 100 to 10 000 nm. Values for typically excitation of Yb^{3+} ions at 976 nm and Nd^{3+} ions are high lighted.[11]

2. Experimental

2.1 Materials

All rare earth chloride hydrates $RECl_3 \cdot xH_2O$ (RE: Y, Yb, Gd, Nd and Er, 99.9%) were purchased from Sigma Aldrich and Alfa Aesar. Ammonium fluoride (NaF, 99.99%), ethanol (absolute) and chloroform (99.8%) were purchased from Sigma Aldrich. Sodium hydroxide (NaCl, 99%) was purchased from Carl Roth and oleic acid (90%) from Alfa Aesar. 2-Aminoethyl dihydrogen phosphate (AEP) (98%) and octadecen (91%) were obtained from Merck. Argon (Ar, 5.0) was received from Praxair and was dried with sicapent. All further chemical reagents used in experiments were directly used without any further purification. For the experiments double distilled water was used.

2.2 Synthesis of $NaYF_4$:Yb^{3+}:Gd^{3+}:Er^{3+} (UCNP) and UCNP:Nd^{3+} ($UCNP_{Nd}$)

The UCNP were synthesized according to a previously reported procedure in which a thermal decomposition method with oleic acid as a capping agent was used.[22,23] The synthesis was designed to keep a constant overall amount of lattice ions (Y^{3+}, Yb^{3+}, Er^{3+}, Nd^{3+}, and Gd^{3+}) in the different samples to study the effect of neodymium. The concentration of the lanthanides (Ln) Er^{3+} and Yb^{3+} was constant for all samples whereas parts of the Y^{3+} ions were replaced by Nd^{3+} ions. $GdCl_3$ hexahydrate (0.61 mmol), $ErCl_3$ (0.06 mmol), $YbCl_3$ (0.34 mmol), $NdCl_3$ (0.02 mmol) and YCl_3 (0.99 mmol) were dissolved under Ar atmosphere in a mixture of oleic acid (13.4 g) and octadecen (35 mL) under stirring. The solution was evacuated (1 mbar) for 45 minutes until evolution of gas had stopped. The reaction mixture was heated to 140 °C under Ar atmosphere until a yellowish clear solution occurs. After the solution had been cooled to 45 °C, ammonium fluoride (300 mg) and sodium hydroxide (150 mg) was added to the reaction mixture under stirring until a clear solution was formed. The solution was heated to 310 °C for 90 minutes using a heating mantle. A discoloration (yellow/brown) of the reaction mixture as well as a white precipitation occurs. When the reaction mixture reached room temperature, the nanoparticles were separated *via* centrifugation (6000 rpm for 25 min) and further purified by several redispersion and centrifugation steps in ethanol. The obtained white powder was dissolved in cyclohexane and filtrated using a 0.2 μm PTFE syringe filter. The as-synthesized UCNPs disperse readily in non polar solvents such as cyclohexane, forming a clear colloidal solution. The oleic acid capped UCNP stored at room temperature were colloidal stable for several months.

2.3 Synthesis of water soluble AEP-capped UCNP

In a typically ligand exchange reaction 150 mg AEP was diluted in solvents mixture of ethanol and ultrapure water (4 mL/6 mL) and 20 mg UCNP dispersed in 5 mL chloroform were added slowly drop wise.[24] The reaction mixture was stirred for 48 h at room temperature, whereas the UCNP moved obviously from the chloroform to the watery phase. After the phase separation the watery phase was centrifuged at 6000 rpm for 25 minutes and the obtained modified UCNP were redispersed in ultrapure water. The AEP-modified UCNP were stored under exclusion of light and different temperature between −10 and 20 °C to get information of the long-term colloidal stability.

2.4 Structural characterization

The size and morphology of as-prepared UCNPs were observed on a JEM 1011 transmission electron microscope (Jeol Ltd, Tokyo, Japan) (TEM) using a wolfram hairpin cathode, an accelerating voltage of 80 kV and a molybdenum panel. The measurements were recorded using a side-mounted Olympus Mega View G2 (Olympus Germany GmbH, Hamburg, Germany). Particle size characterizations were also carried out with dynamic light scattering (DLS) by using a ZETASIZER Nano ZS (Malvern Instruments Ltd, Herrenberg, Germany) as well. As light source a He–Ne laser at $\lambda = 633$ nm was used.

X-ray powder diffraction patterns were obtained using a D5005 (Siemens AG, Munich, Germany) in a range of 3–70°/2θ with divergence aperture, scattering ray aperture and graphite monochromatized Cu Kα radiation (λ = 0.15406 nm). The scanning step was 0.02°/2θ with a counting time of 4 s per step. The nanocrystalline domain sizes were calculated using the Debye–Scherrer equation (eqn (1)):

$$D = \frac{0.89\ \lambda}{B\ \cos(\theta)} \quad (1)$$

D is the domain size to be determined, λ is the wavelength of the X-ray, B is the FWHM of the diffraction peak of interest and θ is the angle of the corresponding diffraction peak.

2.5 Room temperature steady state luminescence spectra

Room temperature (ν = 23 °C) steady state luminescence spectra were obtained using a wavelength tunable pulsed Nd:YAG/OPO laser system (laser: Quanta Ray, Spectra-Physics, Mountain View, CA, USA; OPO: GWU-Lasertechnik Vertriebsges. mbH, Erftstadt, Germany) operating at 10 Hz as excitation light source (at 26 mJ/130 mW) and recorded using an intensified CCD-camera (iStar DH720-18V-73, Andor Technology, Belfast, Great Britain) coupled to a spectrograph (Shamrock SR 303i, Andor Technology, Belfast, Great Britain) equipped with a 600 L mm^{-1} grating blazed at 500 nm.

2.6 Upconversion luminescence measurements at various temperature (288 to 328 K)

In order to study the upconversion luminescence properties at various temperature the experimental set up mentioned above was extended by a water-cooled Peltier element-based temperature adjustable sample holder (temperature controller GR2012 itron 32, JUMO GmbH & Co, Fulda, Germany). In order to ensure the temperature stability the samples were temperated for 15 minutes at the certain temperature. As an additional control a conventional temperature sensor (Testo 945, Testo AG, Lenzkirch, Germany) was used to monitor the temperature of UCNP containing solution under investigation. For all spectroscopic measurements quartz cuvettes sealed with Parafilm® were used.

2.7 Power dependency of upconversion luminescence at room temperature

The intensity of upconversion emission was measured as function of excitation power at $\lambda_{ex} = 976$ nm (further details on equipment *vide supra*). The attenuation of excitation light was achieved by the use of neutral density filters (optical density (OD) 0.1–1.0). The upconversion emission intensity I_{UC} strongly depends on the excitation power I_P (see eqn (2)):[21]

$$I_{UC} \propto (I_P)^n \quad (2)$$

here n is the number of photons required to populate the emitting state of the lanthanides. The power dependence of the Er^{3+} transitions $^2H_{11/2} \rightarrow {}^4I_{15/2}$ (G1), $^4S_{3/2} \rightarrow {}^4I_{15/2}$ (G2) and $^4F_{9/2} \rightarrow {}^4I_{15/2}$ (R) is shown in ESI Fig. 1† using a log I_P − log I_{UC} plot, in which n was calculated from the slope.

3. Results and discussion

3.1 Structural investigations

The particle size and morphology of UCNP and $UCNP_{Nd}$ were studied using TEM, XRD and DLS, respectively. The TEM images of the different UCNP showed that the particles were hexagonal in shape (Fig. 3).[25] In order to determine the average particle size from TEM images approximately 200 particles were included in the statistical analysis (see Table 1).

In addition, DLS and XRD was used as a complementary method for particle size determination. The results of the DLS, TEM and XRD measurements are also shown in Table 1 (see ESI

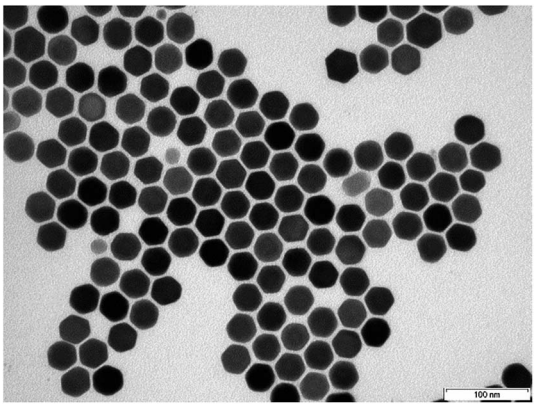

Fig. 3 TEM image of $NaYF_4$:Yb^{3+}:Er^{3+}:Nd^{3+} doped upconversion nanoparticles.

Table 1 Results (full width at halt maximum (FWHM) and particle diameter) of the DLS-, TEM- and XRD analysis of several UCNP synthesis with the same composition and additionally Nd^{3+} doping (n.d.: not determined)

Sample	UCNP	$UCNP_{Nd}$	$UCNP_{Nd,AEP}$
Particle diameter-DLS (nm)	30.2 ± 0.2	29.7 ± 0.1	81.1 ± 0.3
Particle diameter-TEM (nm)	n.d.	34.5 ± 0.1	n.d.
Particle diameter-XRD (nm)	33.9 ± 3.1	32.7 ± 4.2	n.d.
FWHM-DLS	3.3 ± 0.1	3.1 ± 0.1	19.3 ± 0.8
FWHM-TEM	n.d.	1.8 ± 0.3	n.d.

Fig. 2 and 3†). Corroborating the results of the TEM images, DLS and XRD showed as well no particle size alteration upon addition of Nd^{3+}, which was expected due to the very similar atomic radius of the different lanthanides used. Furthermore, it can be assumed that the UCNP/$UCNP_{Nd}$ are highly crystalline, due to the similar particle diameter obtained from TEM/XRD and the fact that only crystalline parts can be observed in XRD. The AEP capped $UCNP_{Nd}$ are 2.7 times larger than the oleic acid capped UCNP, which could be due to the different ligand on the surface resulting in an increase of the hydrodynamic radius or the possible formation of small aggregates. In comparison to the TEM investigations the particle size obtained from the DLS measurements are nearly similar. The deviations in particles size of TEM in comparison to the DLS are due to the fact that calculation algorithm for DLS is optimized for spherical particles whereas variations in shape leads to a change in the scattering behaviour and finally to an inaccuracy in the calculated particle diameter.

3.2 Upconversion luminescence spectroscopy studies

In Fig. 4 the luminescence spectra of the UCNP and $UCNP_{Nd}$ are shown. The optimal excitation wavelengths chosen for the samples under investigation are based on matrices of excitation emission spectra, shown in ESI Fig. 4.† The spectra were recorded in cyclohexane with $\lambda_{ex} = 976$ nm and are the result of energy upconversion processes between Yb^{3+} and Er^{3+} ions (see Scheme 1).[26] The three most intense emission bands can be observed in the green spectral region centered at $\lambda_{em} = 525$ nm ($^2H_{11/2} \rightarrow {}^4I_{15/2}$ transition, G1), 545 nm ($^4S_{3/2} \rightarrow {}^4I_{15/2}$ transition, G2), and in the red spectral region centered at $\lambda_{em} = 660$ nm ($^4F_{9/2} \rightarrow {}^4I_{15/2}$ transition, R).[27–32] The observed fine structure (Stark splitting) is induced by the crystal field splitting due to small differences in the coordination environment.[29,32,33] The Nd^{3+} containing $UCNP_{Nd}$ can be excited at $\lambda_{ex} = 976$ nm and additionally at $\lambda_{ex} = 795$ nm. For the excitation at $\lambda_{ex} = 795$ nm the mechanism of the upconversion processes is extended by an initial energy transfer step between Nd^{3+} and Yb^{3+}. First the Nd^{3+} ions are excited from the $^4I_{9/2}$ to the $^4F_{5/2}$ energy level, followed by a non-radiative relaxation step to $^4F_{3/2}$ level. Originating from this energy level the energy transfer to the $^2F_{5/2}$ level of the Yb^{3+} ions can take place. In such cases the Yb^{3+} acts like a "relay" between the sensitizer Nd^{3+} and the activator Er^{3+}.[1,34–39] The subsequent energy transfer steps and relaxation processes from the Yb^{3+} to the Er^{3+} are identical to the regular UCNP. The cross-relaxation between different excited Er^{3+} ions can be neglected in both cases due to the low Er^{3+} ion concentration used.[31,40] The Gd^{3+} ion doping was chosen to enhance the absolute upconversion luminescence intensity, due to the favoured formation of the β-phase.[41] Since the $^6P_{7/2}$ level, which represents the next electronic state above the ground state of Gd^{3+}, its emission is found in the ultra violet spectral region and is therefore much higher in energy than the relevant excited state levels of Er^{3+}, Nd^{3+}, and Yb^{3+}, respectively. Consequently, a Gd^{3+}-related luminescence quenching by energy transfer of these ions can be ruled out. The upconversion emission spectra ($\lambda_{ex} = 976$ nm) shown in Fig. 3 (right) reveal no significant differences between the UCNP and $UCNP_{Nd}$ investigated, except the G1, G2/R ratio, which is slightly increased. The additional doping of the host lattice with Nd^{3+} ions has no significant impact on the upconversion emission spectra. Also no

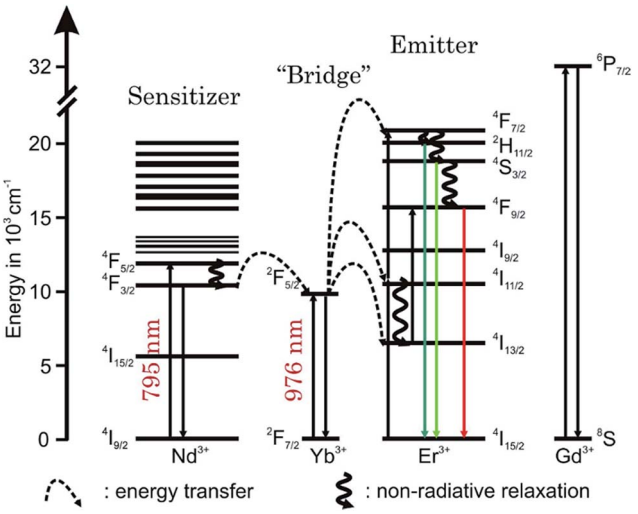

Scheme 1 Schematic energy level diagram of the upconversion mechanism of a Yb^{3+} and Er^{3+} dopant ion system following an excitation at $\lambda_{ex} = 976$ nm. Furthermore, the upconversion mechanism of a Nd^{3+}, Yb^{3+} and Er^{3+} dopant ion system following an excitation at $\lambda_{ex} = 795$ nm is shown as well. The full lines pointing upwards represent energy absorption, the dotted lines represent energy transfer, the waved lines represents non radiative relaxation processes and the colored full lines pointing downwards represents the visible emission.

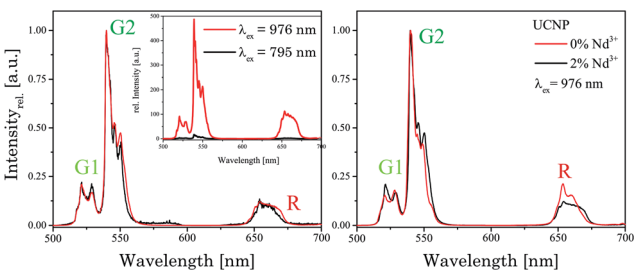

Fig. 4 [Left]: normalized upconversion luminescence spectra of $UCNP_{Nd}$ (in cyclohexane) at $\lambda_{ex} = 976$ nm and 795 nm, respectively. [Inset]: comparison of upconversion emission of $UCNP_{Nd}$ excited at different λ_{ex}. [Right]: typical upconversion emission of UCNP and $UNCP_{Nd}$ excited at $\lambda_{ex} = 976$ nm.

significant differences in the shape or fine structure of the upconversion emission spectra can be seen for different excitation wavelength, due to the fact that the Nd^{3+} ion doping only influence the population of the emitting energy level of Yb^{3+}.

On the other hand the absolute upconversion luminescence intensity is much lower (1/10 intensity) for the excitation at 795 nm (see Fig. 4 inset). The lower upconversion intensity at $\lambda_{ex} = 795$ nm is related to several additional energy transfer steps between Nd^{3+} ions and Yb^{3+} ions as well as relaxation steps of excited Nd^{3+} ions itself. The possibility for non-radiative deactivation channels is increased, subsequently leading to a less effective upconversion.

In Fig. 5 normalized upconversion emission spectra of $UCNP_{Nd}$ with different capping agents at $\lambda_{ex} = 795$ nm as well as 976 nm are shown. The ratio of the emission bands G1, G2 to R is decreased when the nanoparticles are capped with AEP. The change in the G1, G2 to R ratio could be connected to the new chemical environment at the surface of the nanoparticles with different phonon coupling processes influencing the luminescence upconversion. Due to fact that the probability for the non-radiative transition $^4I_{11/2}$ to $^4I_{13/2}$ of Er^{3+} ions is increased, the population efficiency for the energy level R is increased too, whereas of the population of G1 and G2 is decreased, because it is populated by different upconversion mechanisms. The excitation wavelength has no impact on the spectral intensity distribution including the position of the emission bands or emission band ratio as in the case of oleic acid capped UCNP in cyclohexane (see Fig. 4 above).

3.3 Temperature dependent upconversion luminescence

In ESI Fig. 5† emission spectra of UCNP in cyclohexane ($\lambda_{ex} =$ 976 nm) for the temperature range of 288 K < T < 328 K are shown, which are representative for the observed temperature dependence of all UCNP and $UCNP_{Nd}$ investigated.

The following trends were observed for the different luminescence bands of Er^{3+}: (i) the luminescence intensity of the $^2H_{11/2} \rightarrow {}^4I_{15/2}$ transition (G1) gradually increased with increasing temperature and (ii) in contrast to the G1 emission band, the intensity of the G2- and R-related emission bands initially decreased slightly with increasing temperature. The difference in the temperature dependence of the G1 and G2 emission bands is connected to the population pathways of the related energy levels $^2H_{11/2}$ and $^4S_{3/2}$, respectively. In Scheme 2 a detail view of the respective Stark levels of $^2H_{11/2}$ and $^4S_{3/2}$ is shown. The Stark levels are calculated from the excitation and emission spectra of the UCNP under investigation. The population of the green emitting levels G1 and G2 ($^2H_{11/2}$ and $^4S_{3/2}$) usually occurs by successive energy transfer processes from the excited $^2F_{5/2}$ state of Yb^{3+} ions to the Er^{3+} ions exciting it first to the $^4I_{11/2}$ state and in a second step to the $^4F_{7/2}$ excited state. Followed by a non-radiative relaxation process the Er^{3+} ion deactivates to the $^2H_{11/2}$ and – due to the moderate energy gap between $^2H_{11/2}$ and $^4S_{3/2}$ states (about 700 cm^{-1}) – the Er^{3+} ions can relax fast to the $^4S_{3/2}$ state. Finally, the $^2H_{11/2}$ level is repopulated *via* thermal agitation (see Scheme 2) resulting in the observed two Er^{3+}-emission bands G1 and G2 as shown in Fig. 5 (see also Scheme 1).[28–30,42,43]

The thermal equilibration of the two levels is fast, hence the observed intensity ratio of G1 and G2 will be dependent on the temperature.

3.4 UCNP for nanoscale thermometry

For $T > 273$ K the correlation of the luminescence intensity ratio ($Z = I_{G1}/I_{G2}$) and the temperature T can be described by an Arrhenius type equation.[34,35,44]

$$Z = \frac{I_{G1}}{I_{G2}} = A \exp\left(-\frac{\Delta E_{G1/G2}}{k_B T}\right) \quad (3)$$

Z is the ratio of integrated luminescence intensity originating from band G1 and G2 which are separated by the energy gap $\Delta E_{G1/G2}$, k_B is the Boltzmann constant, T is the temperature and A is a constant which depends on the spontaneous emission rate and devolution of the energy levels of the emitting states in the host material. From Fig. 6 (left) it can be seen that Z is changing with temperature, because the relative intensity of the G1-related luminescence is increasing. This is a consequence of

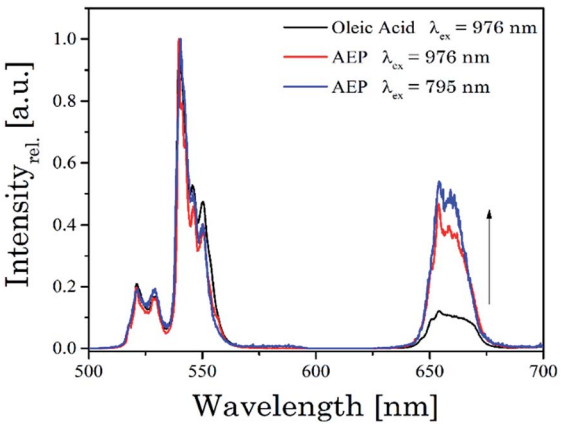

Fig. 5 Normalized upconversion emission spectra of $UCNP_{Nd}$ stabilized with the capping agents oleic acid and AEP. The excitation wavelength λ_{ex} was also varied.

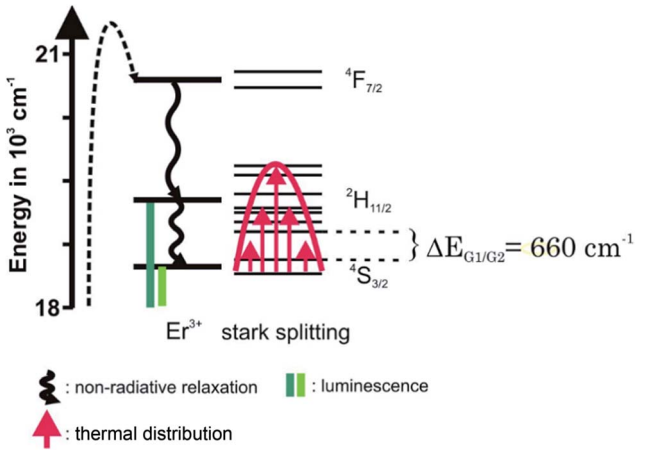

Scheme 2 Close-up of energy levels related to G1 and G2 emission in erbium.

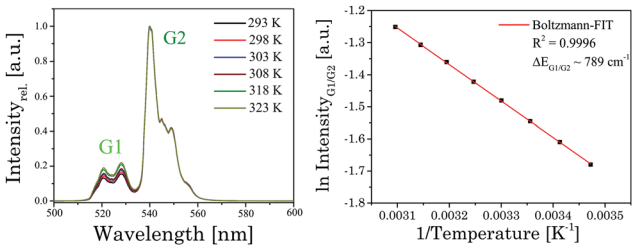

Fig. 6 [Left]: normalized upconversion emission spectra of UCNP at different temperatures. [Right]: analysis of the integrated emission intensity ratio of band G1 and G2 according to eqn (3).

the thermally induced re-distribution in population between the energy levels $^2H_{11/2}$ and $^4S_{3/2}$ (see Scheme 2). Especially for higher temperatures (T > 273 K) a distinct change with temperature was found, which is connected to the fact that the energy gap $\Delta E_{G1/G2}$ is in the order of 600–800 cm^{-1} depending on the host lattice. For UCNP an energy gap $\Delta E_{G1/G2} = 789 \pm 9$ cm^{-1} was determined, which correlates very well with the data of Carnall *et al.* who studied the energy level assignments for Er^{3+} in several host lattices.[42] Based on eqn (3) the absolute sensitivity S_a and relative sensitivity S_r can be obtained.[1,45–48]

$$S_a \sim \left|\frac{\partial Z}{\partial T}\right| \sim Z\,\frac{\Delta E_{G1/G2}}{kT^2} \quad (4)$$

$$S_r \sim 100\%\left|\frac{1}{Z}\frac{\partial Z}{\partial T}\right| \sim 100\%\,\frac{\Delta E_{G1/G2}}{kT^2} \quad (5)$$

The temperature sensitive calculated value of S_a and S_r are shown in Fig. 7. The maximum value of S_r of 1.37% K^{-1} was found at 288 K which is in the range typically found for $NaYF_4$:Yb^{3+}:Er^{3+} or other new host lattices of upconverters like $GdVO_4$:Yb^{3+}:Er^{3+}.[16] The temperature resolution of ~0.4 K was obtained from $\delta R/S_a$ where δR is the standard deviation of the residuals in the polynomial interpolation of the experimental data points (temperature *vs.* $Z = I_{G1}/I_{G2}$). In Table 2 the absolute

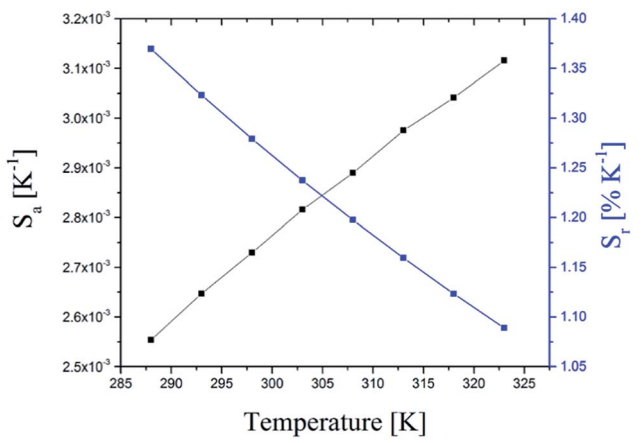

Fig. 7 Absolute (black line) and relative (blue line) sensitivity of the temperature sensor based on Z ($Z = I_{G1}/I_{G2}$) of the upconversion luminescence of UCNPs.

Table 2 Absolute S_a and relative sensitivity S_r of $UCNP_{OA}$ and $UCNP_{AEP}$ at 288 K

Sample	UCNP	UCNP
Capping agent	Oleic acid	AEP
Solvent	Cyclohexane	Water
S_a 10^{-3} [K^{-1}]	2.6	3.0
S_r [% K^{-1}]	1.37	1.38

and relative sensitivity of oleic acid capped UCNP and AEP capped UCNP are shown. It is obvious that the type of ligand and the surrounding medium (cyclohexane and water) has no significant impact on S_a and S_r.

3.5 $UCNP_{Nd}$ as optical probes for thermometry

A big challenge for measurements in "real" biological system are the different optical properties of biological tissues like skin, muscles, connective tissue or vertebral column which only enables a sharp window (700–1000 nm) for optical measurements (see Fig. 8). Based on the water and tissue transmission, which are shown in Fig. 2 and 8, wavelengths around $\lambda_{ex} \sim 800$ nm are more suitable for UCNP based thermometry measurements in contrast to the typical used excitation wavelength of $\lambda_{ex} = 976$ nm, at which also a heating effect by the excitation laser due to water absorption is induced and which is distinctly reduced at $\lambda_{ex} \sim 800$ nm.[13] For UCNP related thermometry the excitation wavelength can be shifted to $\lambda_{ex} \sim 800$ nm upon co-doping with Nd^{3+} (*vide supra*).

The influence of the excitation wavelength on the temperature within the observation volume and near surrounding was monitored using a resistance thermometer in an optical cuvette during the irradiation of the sample with light at $\lambda_{ex} = 795$ nm and 976 nm, respectively (see Fig. 9 and ESI Fig. 6†). It was found that the temperature after irradiation at $\lambda_{ex} = 795$ nm is nearly constant whereas for $\lambda_{ex} = 976$ nm (excitation power ~ 170 mW at both wavelength) an increase in temperature of about $\Delta T \sim$

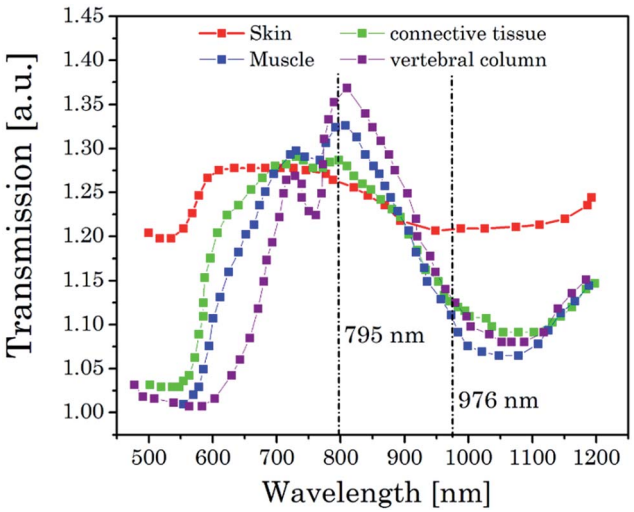

Fig. 8 Transmission spectra of different biological tissue in a spectral range of 500–1200 nm.[13]

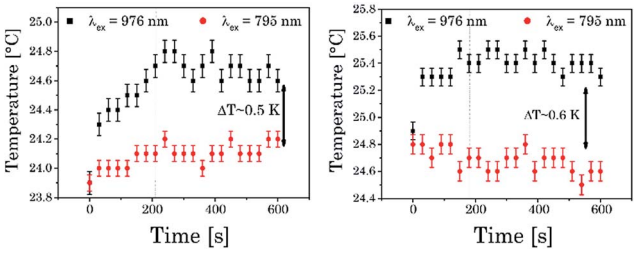

Fig. 9 [Left]: temperature dependence of pure water on the excitation wavelength. [Right]: temperature dependence of $UCNP_{Nd}$ dissolved in water at different at different λ_{ex}.

Table 3 Absolute S_a and relative sensitivity S_r (at 288 K) of $UCNP_{Nd}$. In different solvents excited at 976 nm and 795 nm

λ_{ex} [nm]	976		795	
Solvents	Cyclohexane	Water	Cyclohexane	Water
S_a 10^{-3} [K^{-1}]	2.7	2.9	2.9	3.0
S_r [% K^{-1}]	1.44	1.41	1.31	1.30

0.6 K was found in both cases (pure water and water containing $UCNP_{Nd}$). The maximum ΔT was reached at ~200 seconds of irradiation with $\lambda_{ex} = 976$ nm (since a conventional thermometer was used to measure the temperature change in the nearby bulk phase, the temperature increase at the laser spot is larger).

For biological systems such an increase could induce cellular damage or could significantly influence protein-related processes.[6] On the other hand an excitation wavelength of $\lambda_{ex} = 795$ nm, which is used in the case of $UCNP_{Nd}$, did not show a comparable heating effect in the sample and therefore offers a promising alternative for investigations of biological systems (using UCNP for sensing purposes as well as nanothermometer). As already shown for UCNP (Fig. 6 and 7) the absolute and relative sensitivity of $UCNP_{Nd}$ with different ligands and different excitation wavelength (λ_{ex}) were calculated based on luminescent spectra at different temperatures (see Table 3). The absolute sensitivity is unaffected by the λ_{ex} applied in the measurement and by the solvent. For the relative sensitivity the same was found when comparing the different solvents (for $\lambda_{ex} = 795$ nm S_r was slightly smaller than for $\lambda_{ex} = 976$ nm). The obtained values for S_r are in good agreement with literature data reported for other host materials.[20]

4. Conclusions

The upconversion luminescence properties of oleic acid and AEP stabilized nanoparticles (UCNP) based on a $NaYF_4$ host matrix, which was doped with Yb^{3+} (UCNP) and Yb^{3+}:Nd^{3+} ($UCNP_{Nd}$) as sensitizer and Er^{3+} as activator, respectively, were studied. The focus of this work was the surface modification with AEP to obtain water soluble nanoparticles as well as to investigate possible thermometry applications based on the temperature sensitivity of the upconversion luminescence. The temperature dependence of different luminescence parameters especially the spectral intensity distribution were analysed for the temperature range of 288 K < T < 328 K. Not only the overall luminescence intensity was dependent on the type of capping agent but also the spectral distribution which is effected as well by the phonon coupling possibilities at the surface of the nanoparticles. On the other hand Nd^{3+} ions as additional co-dopant had no effect on the spectral properties of the Er^{3+} related luminescence.

The possibility to excite the UCNP at $\lambda_{ex} = 795$ nm could be realized by the use of Nd^{3+} ions as new sensitizer with no further impact on the spectral distribution. The interplay between spectral distribution and the temperature dependence of photophysical parameters was further investigated. The intensity distribution (*e.g.*, ratio of the green emission G1 and G2) was strongly depending on the temperature and can be used in thermometry applications. In practical applications, efficient collection of fluorescence signal ensures a high signal to noise ratio (SNR) for improving the sensitivity and resolution of QD, fluorescent dyes or upconversion nanoparticle.[49,50] A variety of highly promising approaches of external optical coupling structures for enhancing the excitation and emission of the luminescence from QD or fluorescent dyes are being investigated using cascaded photonic crystal surfaces, which could also be a powerful tool for application based on upconversion nanoparticles.[49,50] Furthermore, the heating effect due to the irradiated excitation light in the observed sample volume was investigated. Whereas for $\lambda_{ex} = 795$ nm only minor increase of the sample temperature was found, the excitation at $\lambda_{ex} = 976$ nm lead to an increase up to 0.6 K which is rather high especially with regards to possible application in biological tissue. In addition to avoiding heating effects the performance of $UCNP_{Nd}$ are comparable to the regular UCNP with respect to absolute and relative sensitivity of temperature sensing. The intensity ratio of the different Er^{3+} luminescence bands in combination with an excitation wavelength of $\lambda_{ex} = 795$ nm can be envisioned to be used as a nanothermometer, *e.g.*, to measure the temperature spatially resolved in tissues with submicron resolution.

Acknowledgements

We are thankful to Dr C. Günter as well as Dr C. Prietzel and Prof. J. Koetz (University of Potsdam) who performed the structural studies (XRD and TEM measurements, respectively) of the samples.

References

1 X.-D. Wang, O. S. Wolfbeis and R. J. Meier, *Chem. Soc. Rev.*, 2013, **42**, 7834.
2 E. F. J. Ring, *Infrared Phys. Technol.*, 2007, **49**, 297–301.
3 J. B. Weaver, *Nat. Nanotechnol.*, 2010, **5**, 630–631.
4 P. R. N. Childs, R. Greenwood and C. A. Long, *Rev. Sci. Instrum.*, 2000, **71**, 2959–2978.
5 C. D. S. Brites, P. P. Lima, N. J. O. Silva, A. Millan, V. S. Amaral, F. Palacio and L. D. Carlos, *Nanoscale*, 2012, **4**, 4799–4829.

6 G. Kucsko, P. C. Maurer, N. Y. Yao, M. Kubo, H. J. Noh, P. K. Lo, H. Park and M. D. Lukin, *Nature*, 2013, **500**, 54–58.
7 K. Okabe, N. Inada, C. Gota, Y. Harada, T. Funatsu and S. Uchiyama, *Nature Commun.*, 2012, **3**, 705.
8 L. Donner, S. Thompson, M. Kreuzer, G. Baffou and R. Quidant, *Nano Lett.*, 2012, **12**, 2107–2111.
9 J. Yang, H. Yang and L. Lin, *ACS Nano*, 2011, **5**, 5067–5071.
10 F. Vetrone, *ACS Nano*, 2010, **4**, 3254–3258.
11 C. Brites, C. P. P. Lima, N. J. O. Silva, A. Millan, V. S. Amaral, F. Palacio and L. D. Carlos, *New J. Chem.*, 2011, **35**, 1177–1183.
12 G. Chen, H. Qiu, P. N. Prasad and X. Chen, *Chem. Rev.*, 2014, **114**, 5161–5214.
13 K. R. Byrnes, R. W. Waynant, I. K. Ilev, X. Wu, K. Smith, R. Heckert, H. Gerst and J. J. Anders, *Lasers Surg. Med.*, 2005, **36**, 171–185.
14 J. Dong and J. I. Zink, *ACS Nano*, 2014, **8**, 5199–5207.
15 A. Sedlmeier, D. E. Achatz, L. H. Fischer, H. H. Gorris and O. S. Wolfbeis, *Nanoscale*, 2012, **4**, 7090–7096.
16 C. Liu, Z. Gao, J. Zeng, Y. Hou, F. Fang, Y. Li, R. Qiao, L. Shen, H. Lei, W. Yang and M. Gao, *ACS Nano*, 2013, **7**, 7227–7240.
17 B. Sikora, K. Fronc, I. Kaminska, K. Koper, S. Szewczyk, B. Paterczyk, T. Wojciechowski, K. Sobczak, R. W. Minikayev, W. Paszkowicz, P. Stepien and D. Elbaum, *Nanotechnology*, 2013, **24**, 235702.
18 G. Shan, R. Weissleder and S. A. Hilderbrand, *Theranostics*, 2013, **3**, 267–274.
19 J. Shen, G. Chen, A.-M. Vu, W. Fan, O. S. Bilsel, C.-C. Chang and G. Han, *Adv. Opt. Mater.*, 2013, **1**, 644–650.
20 T. Gavrilovic, D. Jovanovic, V. Lojpur and M. Dramicanin, *Sci. Rep.*, 2014, **4**, 4209.
21 A. K. Soni, R. Dey and V. K. Rai, *RSC Adv.*, 2015, **5**, 34999–35009.
22 F. Shi and Y. Zhao, *J. Mater Chem. C.*, 2014, **2**, 2198–2203.
23 C. Liu, H. Wang, X. Zhang and D. Chen, *J. Mater. Chem.*, 2009, **19**, 489–496.
24 K. Liu, X. Liu, Q. Zeng, Y. Zhang, L. Tu, T. Liu, X. Kong, Y. Wang, F. Cao, S. A. G. Lambrechts, M. C. G. Aalders and H. Zhang, *ACS Nano*, 2012, **6**, 4054–4062.
25 B. Voß, J. Nordmann, A. Uhl, R. Komban and M. Haase, *Nanoscale*, 2013, **5**, 806–812.
26 F. Wang, R. Deng, J. Wang, Q. Wang, Y. Han, H. Zhu, X. Chen and X. Liu, *Nat. Mater.*, 2011, **10**, 968–973.
27 J. Shan, M. Uddi, N. Yao and Y. Ju, *Adv. Funct. Mater.*, 2010, **20**, 3530–3537.
28 K. Wu, J. Cui, X. Kong and Y. Wang, *J. Appl. Phys.*, 2011, 110.
29 J. Suyver, J. Grimm, K. Krämer and H. Güdel, *J. Lumin.*, 2005, **114**, 53–59.
30 F. Vetrone, J. C. Boyer, J. A. Capobianco, A. Speghini and J. Bettinelli, *J. Phys. Chem. B*, 2003, **107**, 1107–1112.
31 A. Shalav, B. S. Richards, K. Krämer and H. Güdel, *IEEE Photovoltaic Specialists Conference*, 2005, 114–117.
32 J.-C. G. Bünzli and S. V. Eliseeva, *Chem. Soc. Rev.*, 2010, **39**, 189–227.
33 J. M. F. van Dijk and M. F. H. Schuurmans, *J. Chem. Phys.*, 1983, **78**, 5317–5323.
34 Y. Guyot, H. Manaa, J. Y. Rivoire and R. Moncorgé, *Phys. Rev. B: Condens. Matter Mater. Phys.*, 1995, **51**, 784–799.
35 R. Balda, J. I. Pena, M. A. Arriandiaga and J. Fernández, *Opt. Express*, 2010, **18**, 13842–13850.
36 L. Lu, Q. Nie, T. Xu, S. Dai, X. Shen and X. Zhang, *J. Lumin.*, 2007, **126**, 677–681.
37 A. S. Gouveia-Neto, E. B. da Costa, P. V. dos Santos, L. A. Bueno and S. J. L. Ribeiro, *J. Appl. Phys.*, 2003, **94**, 5678.
38 D. Wawrzynczyk, A. Bednarkiewicz, M. Nyk, W. Strek and M. Somac, *Nanoscale*, 2012, **4**, 6959–6961.
39 L. C. Courrol, I. M. Ranieri, L. V. G. Tarelho, S. L. Baldochi, L. Gomes and N. D. V. Junior, *J. Appl. Phys.*, 2005, **98**, 113504.
40 R. B. Anderson, S. J. Smith, P. S. May and M. T. Berry, *J. Phys. Chem. Lett.*, 2014, **5**, 36–42.
41 D. T. Klier and M. U. Kumke, *J. Phys. Chem. C*, 2015, **119**, 3363–3373.
42 W. T. Carnall, P. R. Fields and B. G. Wybourne, *J. Chem. Phys.*, 1965, **42**, 3797–3806.
43 A. Shalav and B. S. Richards, *IEEE Transactions on Electron Devices*, 2007, **54**, 2679–2684.
44 L. H. Fischer, G. S. Harms and O. S. Wolfbeis, *Angew. Chem., Int. Ed.*, 2011, **50**, 4546–4551.
45 C. T. Xu, Q. Zhan, H. Liu, G. Somesfalean, J. Qian, S. He and S. Andersson-Engels, *Laser Photonics Rev.*, 2013, **7**, 663–697.
46 Y. Tian, B. Tian, C. Cui, P. Huang, L. Wang and B. Chen, *Opt. Lett.*, 2014, **39**, 4164–4167.
47 M. Debasu, *Adv. Mater.*, 2013, **25**, 3254–3258.
48 L. Hao and L. Y. Wang, *Chin. Sci. Bull.*, 2013, **58**, 4051–4056.
49 W. Chen, K. D. Long, H. Yu, Y. Tan, J. S. Choi, B. A. Harley and B. T. Cunningham, *Analyst*, 2014, **139**, 5954–5963.
50 Z.-H. Chen, Y. Wang, Y. Yang, N. Qiao, Y. Wang and Z. Yu, *Nanoscale*, 2014, **6**, 14708–14715.

